

# Entanglement spectroscopy of $SU(2)$ -broken phases in two dimensions

F. Kolley,<sup>1</sup> S. Depenbrock,<sup>1</sup> I. P. McCulloch,<sup>2</sup> U. Schollwöck,<sup>1</sup> and V. Alba<sup>1</sup>

<sup>1</sup>*Department of Physics and Arnold Sommerfeld Center for Theoretical Physics,  
Ludwig-Maximilians-Universität München, D-80333 München, Germany*

<sup>2</sup>*School of Physical Sciences, The University of Queensland, Brisbane, QLD 4072, Australia*  
(Dated: September 5, 2018)

In magnetically ordered systems the breaking of  $SU(2)$  symmetry in the thermodynamic limit is associated with the appearance of a special type of low-lying excitations in finite size energy spectra, the so called tower-of-states (TOS). In the present work we numerically demonstrate that there is a correspondence between the  $SU(2)$  tower of states and the lower part of the *ground state* entanglement spectrum (ES). Using state-of-the-art DMRG calculations, we examine the ES of the 2D antiferromagnetic  $J_1$ - $J_2$  Heisenberg model on both the triangular and kagomé lattice. At large ferromagnetic  $J_2$  the model exhibits a magnetically ordered ground state. Correspondingly, its ES contains a family of low-lying levels that are reminiscent of the energy tower of states. Their behavior (level counting, finite size scaling in the thermodynamic limit) sharply reflects TOS features, and is characterized in terms of an effective entanglement Hamiltonian that we provide. At large system sizes TOS levels are divided from the rest by an entanglement gap. Our analysis suggests that (TOS) entanglement spectroscopy provides an alternative tool for detecting and characterizing  $SU(2)$ -broken phases using DMRG.

## I. INTRODUCTION

Recent years have witnessed an increasing interest in entanglement related quantities (and quantum information concepts in general) as new tools to understand the behavior of quantum many body systems [1]. Very recently the entanglement spectrum [2] (ES) has established itself as a new prominent research topic. Considering the bipartition of a system into parts  $A$  and  $B$ , the ES,  $\{\xi_i\}$ , is constructed from the Schmidt decomposition

$$|\psi\rangle = \sum_i e^{-\xi_i/2} |\psi_i^A\rangle \otimes |\psi_i^B\rangle. \quad (1)$$

Here  $|\psi\rangle$  is the ground state, and the states  $|\psi_i^A\rangle$  ( $|\psi_i^B\rangle$ ) provide an orthonormal basis for subsystem  $A$  ( $B$ ). The ES  $\{\xi_i\}$  can also be interpreted as the spectrum of the so called entanglement Hamiltonian  $\mathcal{H}_E \equiv -\log \rho_A$ , where the reduced density matrix  $\rho_A$  is obtained by tracing out part  $B$  in the full system density matrix  $|\psi\rangle\langle\psi|$ .

While in one dimensional (1D) systems the structure of ES is related to integrability [3–5] and (for gapless systems) to conformal invariance [5–8], higher dimensions are by far less explored. In particular, most of the recent literature on two dimensional (2D) systems focused on ES properties in topological phases [2, 9].

In more standard (i.e. non topological) 2D systems, although some results are available [10–13], much less is known. Nevertheless, it has been established recently that in systems displaying ordered ground states (in the thermodynamic limit), with breaking of a *continuous* symmetry, the lower part of the ES is in correspondence with the so called “tower of states” (TOS) spectrum [14, 15]. This describes the low energy structure of *finite size* spectra in systems that spontaneously break a continuous symmetry. In combination with exact diagonalization techniques, tower of states spectroscopy is routinely used to detect symmetry broken phases [16–23].

So far tower of states structures in ES have only been observed numerically in the superfluid phase of the 2D Bose-

Hubbard model [15], where the formation of a Bose condensate is associated with the breaking of a  $U(1)$  gauge symmetry (reflecting conservation of the total number of particles in finite systems). The resulting TOS spectrum, however, (and the lower part of the ES thereof) is “trivial” with one level (excitation) per particle number sector [15].

Richer behavior is expected in  $SU(2)$ -broken phases, where different  $SU(2)$  breaking patterns (i.e. Néel states) give rise to different structures in the energy TOS. For instance, for Néel order with more than two ferromagnetic sublattices (associated with full breaking of  $SU(2)$ ) the spin resolved TOS spectrum exhibits a family of levels (i.e. more than one level) in each spin sector [24].

In this Article we demonstrate that this richer structure is reflected in the lower part of the ES, providing a more stringent check of the correspondence between tower of states and entanglement spectrum. To be specific, we focus on the 2D Heisenberg model with nearest and next-nearest neighbor interaction ( $J_1$  and  $J_2$  respectively). We consider both the kagomé (KHA) and the triangular lattice (THA), restricting ourselves to ferromagnetic  $J_2$  ( $J_2 = -1$ ), to ensure a magnetically ordered ground state on both lattices. In order to take advantage of the  $SU(2)$  invariance of the model we employ non-abelian ( $SU(2)$ -symmetric) DMRG simulations.

Our results are summarized as follows. In both the  $J_1$ - $J_2$  KHA and THA, in the symmetry broken phase, the lower part of the ES (resolved with respect to the block spin  $S_A$ ) sharply reflects the same TOS structure as the physical bulk Hamiltonian. Low-lying ES levels are organized into families, each corresponding to a different  $S_A$  and containing more than one level (in contrast to the Bose-Hubbard model where the TOS structure is “trivial”). The counting of TOS levels in each  $S_A$  sector reflects the corresponding counting in the energy TOS.

The TOS-like structure is divided from higher levels by an entanglement gap, which remains finite (or vanishes logarithmically) in the thermodynamic limit (as found in the Bose-Hubbard ES [15]). All ES levels below the gap are degenerate in the thermodynamic limit, and their finite size behavior is fully understood within the framework of the TOS-ES corre-

spondence. Oppositely, for finite systems, ES levels within each TOS family are not exactly degenerate (similarly to energy TOS [24]) giving rise to intriguing entanglement (TOS) substructures. The main features of TOS levels (TOS substructures, finite size behaviors) are quantitatively characterized by an approximate mapping between the entanglement Hamiltonian and the physical bulk Hamiltonian.

Finally, as an additional point, we investigate the effect of boundary conditions on the TOS structure. To this purpose we consider the ES of the  $J_1$ - $J_2$  KHA ( $J_2/J_1 = -1$ ) on the torus geometry, which has the net effect of introducing two boundaries (edges) between subsystem  $A$  and  $B$ . We find that in  $SU(2)$  broken phases the structure of the ES is weakly affected by boundaries, reflecting the bulk origin of TOS excitations. This is dramatically different in gapped phases [4, 15] or in FQH systems [9] where the ES obtained from bipartitions with multiple edges can be constructed combining single-edge ES.

On the methodological side, our analysis suggests that entanglement TOS spectroscopy, combined with  $SU(2)$  symmetric DMRG, could provide a potentially powerful tool to detect and characterize magnetically ordered ground states. Also, while conventional energy TOS spectroscopy requires the calculation of several excited states (which is computationally expensive in DMRG), ES are readily obtained from *ground state* wavefunctions only.

The Article is organized as follows. Section II introduces the  $J_1$ - $J_2$  Heisenberg model on both the kagomé and triangular lattice. Some basic facts about conventional (energy) tower of states spectroscopy in  $SU(2)$  broken phases are given in section III. In section IV we establish the correspondence between the tower of states and the low-lying part of the ES (cf. IV A). This is numerically verified in IV B for the  $J_1$ - $J_2$  kagomé and triangular lattice Heisenberg model. The fine structure (i.e. entanglement substructures) of ES levels building the TOS is detailed in IV C. Finite size behavior of the (TOS) ES and its dependence on boundary conditions are discussed in section V. Section VI concludes the Article.

## II. MODELS AND METHOD

In this Article we consider the two dimensional spin- $\frac{1}{2}$  Heisenberg model with both nearest and next-nearest neighbor interactions ( $J_1$ - $J_2$ ), defined by the  $SU(2)$  symmetric Hamiltonian

$$\mathcal{H} = J_1 \sum_{\langle ij \rangle} \mathbf{S}_i \cdot \mathbf{S}_j + J_2 \sum_{\langle\langle i, k \rangle\rangle} \mathbf{S}_i \cdot \mathbf{S}_k. \quad (2)$$

Here  $\mathbf{S}_i$  are spin- $\frac{1}{2}$  operators and  $\langle i, j \rangle$ ,  $\langle\langle i, k \rangle\rangle$  denote respectively nearest neighbor and next-nearest neighbor sites on the lattice. We consider both triangular and kagomé cylinders of size  $W \times L$  (Figure 1 (i) and (iii) respectively) with periodic boundary conditions along the vertical direction. We choose  $J_1 > 0$  (antiferromagnetic nearest neighbors interactions) and  $J_2 < 0$  (ferromagnetic next-nearest neighbors interaction). Clearly, a large negative  $J_2$  favors the formation of ferromagnetic sublattices (cf. Figure 1 (i)(iii)) and magnetic order [24].

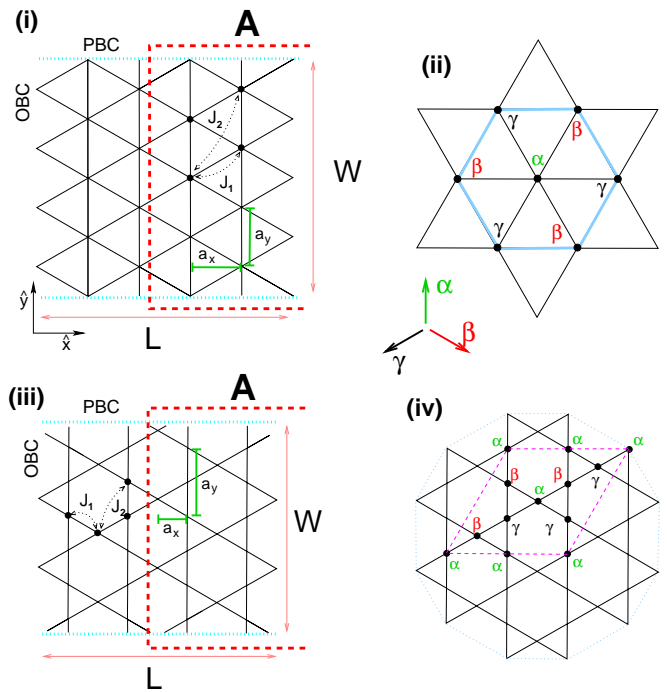


FIG. 1. The  $J_1$ - $J_2$  Heisenberg model on the triangular (THA) and kagomé (KHA) lattice. (i) Example of triangular cylinder of length  $L$  and width  $W$  (measured respectively in units of  $a_x$  and  $a_y$ ). Total number of sites is given as  $W \times L$ . Spins are at the vertices of the lattice. Periodic boundary conditions are used along the vertical direction.  $J_1$  ( $J_2$ ) is the interaction strength between nearest (next-nearest) neighbor spins. In this work we restrict ourselves to anti-ferromagnetic (ferromagnetic)  $J_1$  ( $J_2$ ) (i.e.  $J_1 > 0$ ,  $J_2 < 0$ ). The dashed line is to illustrate the bipartition into two subsystems. (ii) Ordering pattern of the THA. Three possible orientations of the sublattice spins are denoted as  $\alpha$ ,  $\beta$ ,  $\gamma$ . The angle formed by any pair of spins is  $2\pi/3$ . (iii) Heisenberg  $J_1$ - $J_2$  on the kagomé lattice (KHA). Total number of spins is now  $3 \times W \times L$ . (iv) Ordering pattern of the  $J_1$ - $J_2$  KHA ( $\sqrt{3} \times \sqrt{3}$  structure). Dashed line is to highlight the nine spins unit cell.

Here, in particular, we restrict ourselves to  $J_2/J_1 = -1$  to ensure a magnetically ordered ground state on both the triangular and kagomé lattice.

*a. The triangular lattice.*— The ground state of the  $J_1$ - $J_2$  Heisenberg model on the triangular lattice (THA) exhibits at  $J_2/J_1 = -1$  (at a semiclassical level, i.e. considering large spins  $S \gg 1/2$ ) the so called  $120^\circ$  structure. This is depicted in Figure 1 (ii) and consists of three ferromagnetic sublattices (associated with full breaking of spin rotational invariance). Spins on the same sublattice are parallel, while the angle between spins in different sublattices is  $120^\circ$ . A possible choice of ordering pattern is shown in Figure 1 (spin orientations are denoted as  $\alpha$ ,  $\beta$ ,  $\gamma$ ). For spins  $S = 1/2$  (which is the case of interest here) quantum fluctuations are not strong enough to destroy the magnetic order and the  $120^\circ$  structure survives. One should mention that this remains true at arbitrary  $J_2 \leq 0$ , as confirmed by spin-wave calculations [25–30], Green’s function Monte Carlo [31], series expansions [32], tower of states spectroscopy [16], and recent DMRG calcula-

tions [33].

*b. The kagomé lattice.*— Much less is known about the phase diagram of the  $J_1$ - $J_2$  Heisenberg model on the kagomé lattice (KHA) (cf. Figure 1 (iii)). At large ferromagnetic  $J_2 < 0$  (in particular at  $J_2/J_1 = -1$ ) the ground state exhibits magnetic order *à la Néel* with spontaneous breaking of  $SU(2)$  symmetry. The selected ordering pattern is the  $\sqrt{3} \times \sqrt{3}$  state (cf. Figure 1 (iv)). As for the THA (Figure 1 (ii)), three ferromagnetic sublattices are present, although the unit cell (highlighted with the dashed line in the Figure) is now larger (it contains nine spins).

One should mention that, while it is well established that the  $\sqrt{3} \times \sqrt{3}$  order survives at smaller  $J_2$  (i.e. at  $J_2 > -1$ ) [19], it is still a challenging task to determine the phase diagram of the  $J_1$ - $J_2$  KHA in the limit  $J_2 \approx 0$ . In particular, the nature of the ground state of the pure kagomé Heisenberg antiferromagnet (i.e. at  $J_2 = 0, J_1 > 0$ ) is still debated. Several valence bond crystals [34–40] and spin liquid ground states [41–53] (both gapless and gapped) have been proposed. Remarkably, recent state-of-the-art DMRG calculations have provided robust evidence of a gapped  $Z_2$  topological spin liquid [54, 55]. Interestingly, there is also evidence that the spin liquid behavior might survive at small positive  $J_2$  with the formation of an extended spin liquid region [56].

*c. Entanglement spectrum (ES).*— In order to calculate the ES we consider the bipartition of the system (cylinders in Figure 1) into two equal parts  $A$  and  $B$ , using a vertical cut (dashed line along the  $y$ -direction in Figure 1 (i)(iii)). As a consequence, the boundary between  $A$  and  $B$  is a circumference of length  $W$ . The total subsystem spin  $\mathbf{S}_A^2$  is a good “quantum number” for the ES and can be used to label ES levels (i.e. ES levels are organized into  $SU(2)$  multiplets). Equivalently, the entanglement Hamiltonian  $\mathcal{H}_E$  (or the reduced density matrix  $\rho_A$ ) exhibits a block structure, each block corresponding to a different  $\mathbf{S}_A$  sector.

*d. Ground state search (DMRG method).*— The ground state is obtained in a matrix product state form by using state-of-the-art  $SU(2)$ -symmetric single-site DMRG [57–59]. DMRG (Density Matrix Renormalization Group) is a variational method in the ansatz space spanned by matrix product states (MPS). The method allows one to find the ground state of one-dimensional (1D) systems efficiently even for large system sizes. It has also been successfully applied to two-dimensional (2D) lattices by mapping the short-ranged 2D Hamiltonian exactly to a long-ranged 1D one [33, 54, 55, 60–63]. Here, to ensure independence on the actual mapping, we performed several calculations using different mappings. DMRG computational cost scales roughly exponentially with the entanglement entropy and favors open (OBC) over periodic boundary conditions (PBC). The conventional compromise, taken also by us, is to consider cylinders, i.e. PBC along the short direction (circumference  $W$ ) and OBC along the long direction (length  $L$ ) where boundary effects are less important. Computational cost is then dominated exponentially by  $W$ . Exploiting the power of the non-abelian formulation we were able to simulate the systems using up to 5,000 ansatz states, corresponding to roughly 20,000 states in an abelian  $U(1)$  DMRG, allowing us to obtain the ground

state of (2) with high accuracy, even for cylinders with  $W = 9$  (for the  $J_1$ - $J_2$  THA) or fully periodic tori. One should also mention that in  $SU(2)$ -broken phases the large entanglement gap, which divides the TOS ES levels from the rest, reduces significantly the effective number of states needed to get well converged ground states.

### III. TOWER OF STATES SPECTROSCOPY IN $SU(2)$ BROKEN PHASES

Due to its manifest spin rotational invariance, the finite size spectrum of (2) can be decomposed into the irreducible representations of  $SU(2)$ , using the eigenvalue  $S$  of the total spin  $\mathbf{S}^2$  to label energy levels (and eigenstates). The resulting spin-resolved spectrum shows striking signatures of the  $SU(2)$  breaking (happening in the thermodynamic limit). Exact diagonalization studies [19] demonstrated that at  $J_2/J_1 = -1$  in each spin sector  $S$  there is a family of (low-lying) levels, which are clearly separated from the rest by an energy gap (at least for large systems). These are called “quasidegenerate joint states” (QDJS) in Ref. [17] and form the “tower of states” (TOS) structure.

The number  $N_S$  of TOS levels in each spin sector is related to the Néel state selected in the thermodynamic limit. For instance, Néel ordering with two ferromagnetic sublattices (as for the Heisenberg antiferromagnet on the square lattice [24]), corresponding to the breaking of  $SU(2)$  down to  $U(1)$ , implies  $N_S = 2S + 1$ . On the other hand, a complete breaking of  $SU(2)$  (for instance Néel ordering with more than two ferromagnetic sublattices, as for both the THA and KHA, cf. Figure 1) implies  $N_S > 2S + 1$  [24] (see also below).

The TOS structure can be obtained as the lowest energy manifold of an effective Hamiltonian  $\mathcal{H}_T$  (“quantum top”), which, for Néel order with three ferromagnetic sublattices  $a, b, c$ , reads [16, 64–67]

$$\mathcal{H}_T = \frac{1}{2\chi V} (\mathbf{S}^2 - \mathbf{S}_a^2 - \mathbf{S}_b^2 - \mathbf{S}_c^2) \equiv \frac{1}{\chi V} (\mathbf{S}_a \cdot \mathbf{S}_b + \mathbf{S}_a \cdot \mathbf{S}_c + \mathbf{S}_b \cdot \mathbf{S}_c). \quad (3)$$

Here  $\chi$  is the spin susceptibility,  $V$  the volume (i.e. total number of sites), and  $\mathbf{S}$  ( $\mathbf{S}_{a,b,c}$ ) the total spin of the system (sublattice). Notice that one could think of (3) as an effective Heisenberg coupling between  $\mathbf{S}_a, \mathbf{S}_b, \mathbf{S}_c$ , acting as collective degrees of freedom. As the lowest energy manifold of (3) is obtained choosing  $S_a = S_b = S_c = V/3 \times 1/2$ , one readily obtains the number of TOS levels per spin sector as  $N_S = (2S + 1)^2$  [17]. These, according to (3), are degenerate with energy given as

$$E_T(S) = \frac{1}{2\chi V} S(S + 1), \quad (4)$$

where we neglected the sublattice contributions, keeping only  $S$  dependent terms. Plotted as function of  $S(S + 1)$ , TOS levels show the typical “Pisa tower” (linear) structure [17], with a vanishing (as  $1/V$ ) “slope”.

Still, one should think of (3) only as the low energy approximation of (2). To go beyond one can split  $\mathcal{H}$  as  $\mathcal{H} = \mathcal{H}_T + \mathcal{H}'$

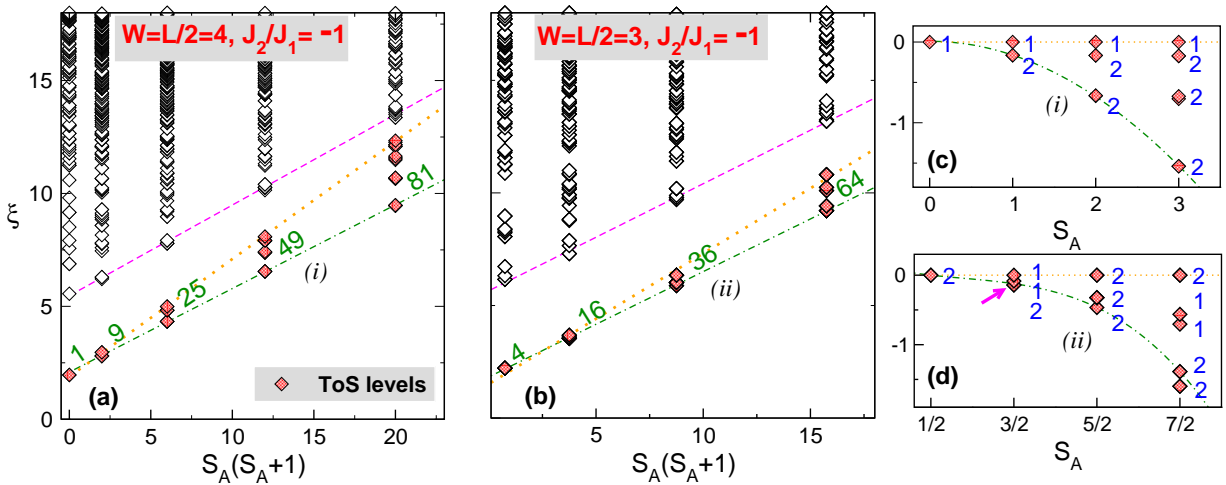


FIG. 2. Tower of states (TOS) structure in the ES of the  $J_1$ - $J_2$  kagomé Heisenberg model (KHA) at  $J_2/J_1 = -1$ . Half-system ES levels  $\xi$  versus  $S_A(S_A + 1)$ , with  $S_A$  the block spin. Symbols are DMRG data for the KHA on a cylinder with  $W = L/2 = 4$  (cf. (a)) and  $W = L/2 = 3$  (cf. (b)), same scale used on the  $y$ -axis. Each point corresponds to a degenerate  $SU(2)$  multiplet ( $2S_A + 1$  levels). Filled symbols denote levels building the TOS. Dashed-dotted line is to highlight the behavior as  $S_A(S_A + 1)$ . TOS levels are divided from the rest (levels above the dashed line in the Figure) by an entanglement gap. Accompanying numbers are the numbers of TOS ES levels. Right panels (c)(d): Enlarged view of the TOS structures (i)(ii) shown respectively in (a) and (b). In each  $S_A$  sector ES levels are shifted by the value of the highest level (dotted line in (a)(b)). ES levels are plotted against the block spin  $S_A$ . The number of degenerate  $SU(2)$  multiplets is reported in blue. In (d) the arrow is to stress the presence of isolated (i.e. unpaired) multiplets (see also multiplets at  $S_A = 7/2$ ).

with  $\mathcal{H}'$  a (higher energy) correction to  $\mathcal{H}_T$ . Specifically, one has  $\mathcal{H}' \approx \mathcal{H}_{sw}$ ,  $\mathcal{H}_{sw}$  describing levels immediately above the TOS structure. These correspond to spin waves (Goldstone modes) and possess a linear dispersion, implying (using that momentum is discretized on a finite lattice as  $1/\sqrt{V}$ )  $\mathcal{H}_{sw} \approx 1/\sqrt{V}$ . As a striking consequence the TOS spectrum (4) is divided from higher energy levels by an apparent gap at  $V \rightarrow \infty$ .

Moreover, since in general  $[\mathcal{H}_T, \mathcal{H}'] \neq 0$ , the degeneracy within each TOS manifold at spin  $S$  (cf. (4)) is partly lifted, implying that  $\mathcal{H}_T$  (cf. (3)) has to be modified. Notice that, in principle, the final degeneracy structure can be predicted using group symmetry analysis [17]. Remarkably, in the limit of large systems  $\mathcal{H}_T$  can be mapped to the anisotropic “quantum top” [17]

$$\mathcal{H}_T = \frac{\mathbf{S}^2}{2V\chi_{\perp}} + \frac{(S^{z'})^2}{2V} \left( \frac{1}{\chi_{\parallel}} - \frac{1}{\chi_{\perp}} \right). \quad (5)$$

Here  $S^{z'} \in [-S, S]$  is the component of the total spin along the third axis  $z'$  of the “quantum top” (not necessarily the  $z$  axis in the lab-frame), while  $\chi_{\parallel}$  and  $\chi_{\perp}$  denote respectively the parallel and transverse susceptibilities, which measure the response to magnetic fields in the plane of the spins and in the perpendicular one. Notice that both terms in (5) are  $\sim 1/V$ . One has for large system sizes  $\chi_{\perp} \neq \chi_{\parallel}$ , reflecting the tendency towards magnetic order and the system response becoming anisotropic. The degeneracy structure of TOS multiplets is now readily obtained from (5): in the sector with half-integer  $S$  there are  $S + 1/2$  pairs of degenerate multiplets, whereas for integer  $S$  one has  $S$  degenerate pairs and an extra isolated multiplet (corresponding to  $S^{z'} = 0$  in (5)).

#### IV. ENTANGLEMENT SPECTRA IN $SU(2)$ -BROKEN PHASES

In this section we numerically demonstrate that in  $SU(2)$ -broken phases the information contained in the energy tower of states (TOS) is nicely embodied in the lower part of the ground state entanglement spectrum (TOS-ES correspondence). This section is organized as follows. In IV A we establish the TOS-ES correspondence [14, 15], which is expressed as a mapping between the TOS Hamiltonian  $\mathcal{H}_T$  and the entanglement Hamiltonian  $\mathcal{H}_E$ . This is supported numerically in IV B highlighting TOS structures in the ES of the  $J_1$ - $J_2$  KHA and THA (at  $J_2/J_1 = -1$ ). Our main results are illustrated in Figure 2 and 3. Finally, the fine structure (TOS substructure) of the TOS-related levels is detailed in IV C.

##### A. TOS-ES correspondence

It has been suggested recently that in systems breaking a *continuous* symmetry in the thermodynamic limit the lower part of the (ground state) ES has the same structure as the TOS energy spectrum [14]. Here we restrict ourselves to the situation of  $SU(2)$  symmetry breaking. The correspondence can be expressed as a mapping between an effective entanglement Hamiltonian  $\mathcal{H}_E$  (describing the lower part of the ES) and the TOS Hamiltonian  $\mathcal{H}_T$ . Specifically, one has [14]

$$\mathcal{H}_E \propto \mathcal{H}_T(A)/T_E, \quad (6)$$

where  $\mathcal{H}_T$  is restricted to the degrees of freedom of subsystem  $A$  and  $T_E \approx v_s/\sqrt{V}$  is an effective “entanglement temperature”, which reflects the presence of gapless excitations (spin

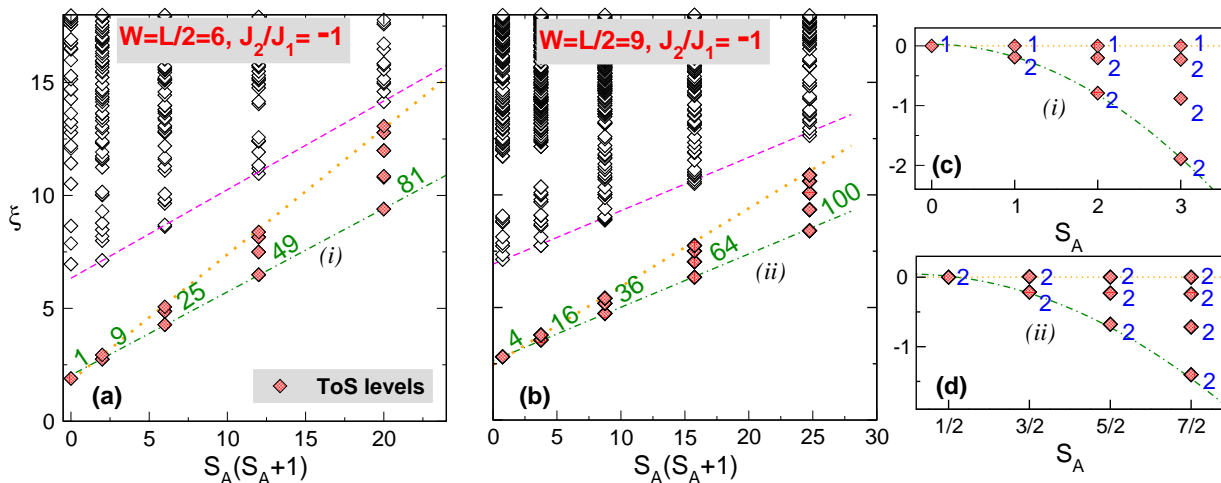


FIG. 3. Tower of states (TOS) structure in the ES of the  $J_1$ - $J_2$  Heisenberg model on the triangular lattice (THA) ( $J_2/J_1 = -1$ ). ES for half of the system: ES levels  $\xi$  versus  $S_A(S_A + 1)$ ,  $S_A$  being the total subsystem spin. Symbols are DMRG data for cylinders with  $W = L/2 = 6$  (a) and  $W = L/2 = 9$  (b) (cf. Figure 1). Each point corresponds to a degenerate  $SU(2)$  multiplet ( $2S_A + 1$  levels). Filled symbols denote the ES levels forming the TOS. Dashed-dotted line highlights the TOS behavior as  $S_A(S_A + 1)$ . TOS levels are divided from the rest of the spectrum (levels above the dashed line) by an entanglement gap. The total number of ES levels in each  $S_A$  sector is reported in green (numbers accompanying ES multiplets). Right panel: Enlarged view of the TOS structures in (a) and (b), ES plotted versus  $S_A$ . ES levels at each  $S_A$  are shifted by the highest level (dotted lines in (a)(b)). Lines are guides to the eye as in (a)(b). Accompanying numbers denote the number of degenerate multiplets.

waves) arising from the breaking of the  $SU(2)$  symmetry (here  $v_s$  is the spin wave velocity). The behavior  $T_E \approx 1/\sqrt{V}$  originates from the linear dispersion of spin waves and the momentum quantization as  $1/\sqrt{V}$  on a finite lattice.

From (6) two remarkable properties can be derived. First, using that  $\mathcal{H}_T \sim 1/V$  (cf. (5)) and  $T_E \sim 1/\sqrt{V}$ , one obtains that the spacing between the ES levels building the TOS structure is vanishing as  $1/\sqrt{V}$  in the thermodynamic limit. Additionally, including the spin wave contributions in the energy spectrum, i.e. replacing  $\mathcal{H}_T \rightarrow \mathcal{H}_T + \mathcal{H}_{sw}$ , and assuming that ES levels above the TOS structure are spin wave like, from (6) one obtains  $\mathcal{H}_E$  as

$$\mathcal{H}_E \sim (\mathcal{H}_T + \mathcal{H}_{sw})/T_E. \quad (7)$$

The behaviors  $T_E \sim 1/\sqrt{V}$  and  $\mathcal{H}_{sw} \sim 1/\sqrt{V}$  now suggest the formation of a finite gap (in the limit  $V \rightarrow \infty$ ) between the TOS structure and the higher part of the ES. However, one should stress that a logarithmic vanishing of the entanglement gap, also suggested by field theoretical calculations [68], cannot be excluded. These findings (presence of a finite gap in the ES and the finite size behavior of the TOS structure) have been confirmed in Ref. [15] for the 2D Bose-Hubbard model in the superfluid phase.

Finally, it is interesting to discuss how TOS structures affect the behavior of the entanglement entropy. The fact that the low-energy part of (2) (and its ground state) can be described by an effective free bosonic theory ( $\mathcal{H}_{sw}$ , cf. section III) suggests that an area law behavior should be expected (cf. [1] and references therein for a discussion of area laws in free systems). On the other hand, the breaking of a continuous symmetry gives rise to additive logarithmic corrections to the entropy [14], which, for instance, have been observed nu-

merically in the 2D Heisenberg antiferromagnet on the square lattice [69–71]. At the level of the ES, these corrections are associated with the TOS structure, while the area law arises from ES levels above the entanglement gap. Note that the entanglement gap is typically large deep in a  $SU(2)$ -broken phase (see section IV B), implying that the TOS levels give the dominant contribution to the entanglement entropy, while the area law behavior is recovered only asymptotically for large system sizes.

## B. DMRG results

*$J_1$ - $J_2$  kagomé Heisenberg (KHA).*— We start discussing the tower of states structures in the ES of the KHA at  $J_2/J_1 = -1$ . Figure 2 plots the ES (DMRG data) obtained from the ground state of the KHA on cylinders (cf. Figure 1 (iii)) with fixed aspect ratio  $W/L = 1/2$  and  $W = 3, 4$  (respectively center and left panels in Figure 2). Total number of spins in the subsystem is given as  $3W^2$  (ES is for half cylinder) and is even (odd) for  $W = 4(3)$ . ES levels  $\xi$  are plotted versus  $S_A(S_A + 1)$ ,  $S_A$  being the total spin of subsystem  $A$ .

In each spin sector  $S_A$  a family of low-lying ES multiplets (each point corresponds to an  $SU(2)$  multiplet of degenerate levels, filled rhombi in Figure 2) is well separated from higher levels by a gap. The total number of levels below the gap (TOS levels) in each sector  $S_A$  is given as  $(2S_A + 1)^2$  (numbers accompanying ES multiplets in the Figure), clearly reflecting the corresponding multiplicity (as  $(2S + 1)^2$  in the energy tower of states (cf. section III)). Also, the lower part of the TOS levels exhibits the typical TOS behavior as  $S_A(S_A + 1)$  (see dashed-dotted lines in Figure 2) in agree-

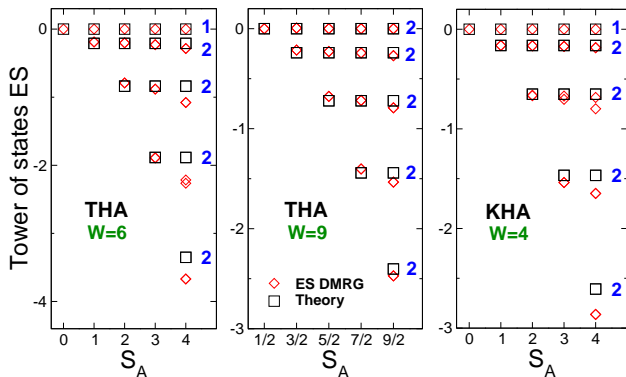


FIG. 4. TOS entanglement substructures. ES of the Heisenberg  $J_1$ - $J_2$  model on the triangular (THA) and kagomé (KHA) lattice: ES levels  $\xi$  versus the total spin  $S_A$  of subsystem  $A$ . Each point corresponds to a degenerate  $SU(2)$  multiplet ( $2S_A + 1$  levels). Only multiplets building the TOS structure are shown. In each spin sector with fixed  $S_A$  ES multiplets are shifted by the value of the largest level. Rhombi are the same DMRG data as in Figure 2 and 3 panels (c)(d)). The squares denote the (one parameter) fit to the theoretical prediction (cf. (8)) in the limit of large systems ( $W, L \rightarrow \infty$ ). In all panels accompanying numbers denote the number of degenerate  $SU(2)$  multiplets.

ment with (4) and (6). The entanglement gap appears to be constant as a function of  $S_A$  (dashed line denotes levels immediately above the TOS structure), similarly to what is observed in energy TOS structures [24] and in the ES of the 2D Bose-Hubbard [15].

Interestingly, at each fixed  $S_A$  the TOS levels are not exactly degenerate, and further substructures appear, reflecting the presence of the second term in (5). TOS substructures are better highlighted in Figure 2 (c)(d) showing an enlarged view of the TOS levels (same DMRG data as in panels (a)(b)). In each sector  $S_A$  we shifted the ES by subtracting the value of the largest level (dashed-dotted and dashed lines are guides to the eye as in panels (a)(b)). Reported numbers correspond now to the number of degenerate  $SU(2)$  multiplets.

According to (6) the degeneracy structure in the TOS part of the ES is the same as that in the energy tower of states. At large system sizes and *integer*  $S_A$  (i.e. even number of spins in  $A$ ) the TOS ES levels are organized in pairs of degenerate multiplets, apart from one isolated multiplet at the top of each  $S_A$  sector. This is clearly supported in Figure 2 panel (c).

On the other hand, for *half-integer*  $S_A$  only pairs of degenerate multiplets are expected (cf. (5)). Figure 2 (d) shows the TOS ES levels for the kagomé cylinder with  $W = 3$  (i.e. 27 spins in subsystem  $A$ ). Although a clear tendency towards the formation of pairs is visible (levels at the top of the structure form pairs, while in panel (c) one has one isolated multiplet), some deviations are observed. For instance (see arrow in Figure 2 (d)), one has in the sector with  $S_A = 3/2$  four  $SU(2)$  multiplets, but only two form a pair. Similarly, in the sector with  $S_A = 7/2$  two isolated multiplets are visible. Since (5) is valid only in the asymptotic (i.e. large  $V$ ) regime, these deviations have to be understood as finite size effects. Indeed, we checked that at  $W = 5$  (i.e. 75 spins in subsystem  $A$ ) all

the (TOS) multiplets form degenerate pairs (at least in the first few  $S_A$  sectors).

*$J_1$ - $J_2$  triangular Heisenberg (THA).*— Further evidence supporting the TOS-ES scenario is provided in Figure 3 considering the 2D  $J_1$ - $J_2$  Heisenberg model on the triangular lattice (THA). The ground state ordering pattern ( $120^\circ$  structure, cf. Figure 1 (ii)) contains three ferromagnetic sublattices (full breaking of  $SU(2)$ ) and the same tower of states structure as for the kagomé is expected.

Figure 3 plots DMRG data for the ES of the THA on the cylinder (at fixed aspect ratio  $W/L = 1/2$  with  $W = 6$  and  $W = 9$ , respectively in panel (a) and (b)). ES is for half of the cylinder. Notice that we could access larger system sizes than for the kagomé (compare with Figure 2). This allows us to resolve the TOS multiplets (corresponding to 100 ES levels) at  $S_A = 9/2$ . As for the kagomé ES (cf. Figure 2) the lower part of the ES (filled symbols in the Figure) is divided from the rest of the spectrum by an entanglement gap and exhibits the typical TOS behavior as  $S_A(S_A + 1)$ .

The correct  $SU(2)$  TOS level counting (i.e. number of TOS levels in each spin sector  $S_A$ ) as  $(2S_A + 1)^2$  is fully reproduced. The fine structure of TOS multiplets (TOS substructure) is highlighted in Figure 3 (c)(d). Remarkably, for odd number of spins in  $A$  all TOS levels are organized into pairs of degenerate multiplets (cf. Figure 3 (d)), whereas for even ones there is an isolated ES multiplet at the top of the structure (cf. Figure 3 (c)), signaling that finite size corrections are somehow smaller than in the kagomé ES (cf. Figure 2).

### C. Tower of states entanglement substructures

We now analyze quantitatively the structure of the TOS ES multiplets. We start with observing that in the limit of large cylinders the effective entanglement Hamiltonian  $\mathcal{H}_E$  describing the TOS structure is obtained from (5) and (6) as

$$\mathcal{H}_E \sim \frac{S_A^2}{v_s \chi_\perp W} - \frac{(S_A^{z'})^2}{v_s W} \left( \frac{1}{\chi_\perp} - \frac{1}{\chi_\parallel} \right), \quad (8)$$

where we used that  $\sqrt{V} \approx W$ . While the first term in (8) gives the TOS behavior as  $S_A(S_A + 1)$  (cf. Figure 2 and 3), with  $(2S_A + 1)^2$  *degenerate* levels at each  $S_A$ , the second gives rise to the substructures in Figure 2 and 3 (c)(d).

These are shown in Figure 4 plotting the shifted ES levels (same DMRG data as in Figure 2 and 3 panels (c)(d)) for both the triangular and kagomé  $J_1$ - $J_2$  Heisenberg model at  $J_2/J_1 = -1$ . Since ES levels in each sector  $S_A$  are shifted by the value of the largest level, the contribution of the first term ( $\sim S_A(S_A + 1)$ ) in (8) has to be neglected. Thus, structures appearing in Figure 4 are described by  $\alpha[(S_A^{z'})^2 + s_0]$ , being  $\alpha \sim (\chi_\parallel - \chi_\perp)/(v_s W \chi_\perp \chi_\parallel)$ , and  $s_0 = 0(-1/4)$  for integer(half-integer) values of  $S_A$ .

This scenario is confirmed fitting TOS levels in Figure 4 to  $\alpha[(S_A^{z'})^2 + s_0]$ , with  $\alpha$  the only fitting parameter. For the THA (including in the fit only the ES towers with  $S_A \leq 3$ ) it is  $\alpha \approx 0.21$ , while for  $W = 9$  (now including all the ES levels with  $S_A \leq 9/2$ ) one obtains  $\alpha \approx 0.12$ . Notice that it is

$0.12/0.21 \sim 0.6 \sim 2/3$ , supporting the behavior  $\alpha \sim 1/W$  (cf. (8) and section V). For the KHA ( $W = 4$ ) a similar fit gives  $\alpha \approx 0.17$ , (only ES levels with  $S_A \leq 3$  were fitted). Results of the fit are shown in Figure 4 as squares and are in excellent agreement with the DMRG data. Also, the agreement is better at larger system sizes (compare in Figure 4 DMRG data for the THA at  $W = 9$  and  $W = 6$ ), confirming that (8) holds in the asymptotic regime  $V \rightarrow \infty$ .

## V. FINITE SIZE AND BOUNDARY EFFECTS IN TOS STRUCTURES

One crucial consequence of the correspondence between TOS and entanglement spectra, according to (8), is that the spacing within low-lying ES multiplets is  $\sim 1/\sqrt{V} \approx 1/W$ . Oppositely, the entanglement gap between the TOS part and the rest of the spectrum remains finite in the thermodynamic limit (or vanishes logarithmically, cf. the discussion in section IV A). These features are numerically demonstrated in V A.

The effect of boundary conditions on TOS structures is instead discussed in V B, by examining the ES of the  $J_1$ - $J_2$  KHA on the torus. The most notable consequence of the torus geometry is that the number of boundaries between the two subsystems is doubled. However, although this gives rise to quantitative differences compared to the cylinder geometry, qualitative features (i.e. TOS behavior as  $S_A(S_A + 1)$  and TOS multiplets counting) remain unchanged, signaling the bulk origin of the TOS structures.

### A. Entanglement gap & TOS level spacing: finite size scaling analysis

The structure of the lower part of the ES (TOS structure) can be characterized using the entanglement gap  $\Delta_0$  and the tower of states level spacing  $\delta$  [15]. These are defined pictorially in Figure 5 (a). More formally,  $\delta$  is the “distance” between the two lowest levels in the sectors with  $S_A = 0, 1$  (respectively  $S_A = 1/2, 3/2$  for  $S_A$  half integer), i.e.  $\delta \equiv \xi_1 - \xi_0$  with  $\xi_\sigma$  the lowest ES level in the sector with  $S_A = \sigma$ . This is also a measure of the “slope” of the TOS structure. The entanglement gap  $\Delta_0$  measures, instead, the separation between the TOS structure and the higher ES levels. Since it depends weakly on  $S_A$  (cf. Figure 2 and 3), here we consider the gap  $\Delta_0$  in the lowest spin sector ( $S_A = 0(1/2)$  for integer (half-integer)  $S_A$ ).

Figure 5 (b) plots  $\Delta_0$  as function of the boundary length  $2 \leq W \leq 9$  for both the kagomé and triangular  $J_1$ - $J_2$  Heisenberg model ( $J_2/J_1 = -1$ ). The ES is for half of the system and data is DMRG for cylinders with fixed aspect ratio  $W/L = 1/2$ . For both models the extrapolation to infinite cylinders (assuming the behavior  $1/\sqrt{V} \sim 1/W$ ) (dotted lines) suggests a finite value (crosses in the Figure) of  $\Delta_0$  (see, however, the discussion in IV A).

Figure 5 (c) shows  $\delta$  versus  $1/W$ . In order to avoid parity effects (in  $V$ ) we plot  $\delta/dS_A^2$ , with  $dS_A^2 \equiv S_A(S_A + 1)|_1 -$

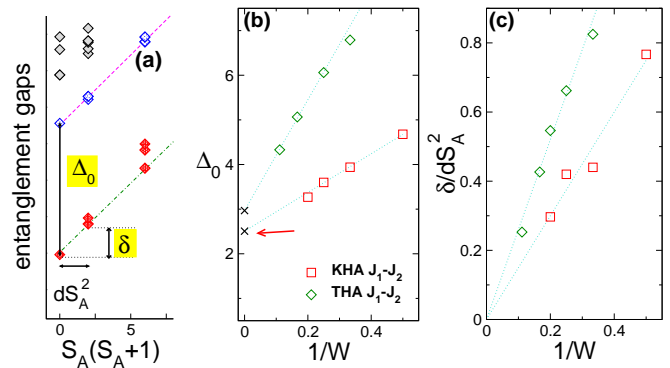


FIG. 5. Finite size scaling of the entanglement gap  $\Delta_0$  and the tower of states spacing  $\delta$  in the  $J_1$ - $J_2$  Heisenberg model on the kagome (KHA) and triangular (THA) lattice (at  $J_2/J_1 = -1$ ). DMRG data for the ES of half the system (cylindrical geometry as in Figure 1 with fixed aspect ratio  $W/L = 1/2$ ). (a) Pictorial definitions of entanglement gap and tower level spacing:  $\delta$  is the “distance” between the two lowest levels in the ES (here respectively in the sectors  $S_A = 0$  and  $S_A = 1$ ).  $\Delta_0$  is the gap between the TOS structure and higher ES levels in the  $S_A = 0$  sector. (b)  $\Delta_0$  as function of  $1/W$ : the gap is finite in the limit  $W \rightarrow \infty$ . Dotted lines are fits to  $A + B/W$ . The extrapolated values for  $A$  are shown as crosses. (c) Vanishing of the tower level spacing  $\delta$  in the thermodynamic limit. To avoid odd-even effects  $\delta$  is divided by  $dS_A^2 = 2, 3$  for respectively integer and half-integer  $S_A$ .  $\delta/dS_A^2$  plotted versus  $1/W$ . Dotted lines are fits to  $A/W$ .

$S_A(S_A + 1)|_0$ . Clearly, this is vanishing for infinite cylinders ( $W \rightarrow \infty$ ). The expected behavior  $\delta \sim 1/\sqrt{V} \sim 1/W$  (cf. (8)) is fully confirmed for the  $J_1$ - $J_2$  THA (rhombi in the Figure, dotted line is a fit to  $A/W$ ), while for the  $J_1$ - $J_2$  KHA the scenario is less robust due to residual parity effects.

### B. Periodic boundary conditions: ES of the KHA on the torus

Boundary conditions, in particular number of boundaries between the two subsystems, can affect dramatically the ES (and the entanglement entropies). For instance, in gapped (non-topological) one dimensional and two dimensional systems the ES is a boundary local quantity [4, 15] and a change in the number of boundaries leads to quantitative and qualitative changes in the ES. It is interesting to clarify the effect of boundary conditions on the TOS structures outlined in IV. To this purpose here we consider the ES of the  $J_1$ - $J_2$  KHA on the torus.

This is illustrated in Figure 6 (ES for half-torus, DMRG data at  $J_2/J_1 = -1$ ). Data points are for both  $W = 3$  and  $W = 4$  (at fixed aspect ratio  $W/L = 1/2$ , respectively (a) and (b) in Figure 6). The main features of low-lying ES multiplets are the same as in the cylindrical geometry (compare Figure 6 with Figure 2). The linear behavior of the ES as function of  $S_A(S_A + 1)$  (Pisa tower structure) is clearly visible and an apparent gap divides the low-lying ES multiplets from the rest. The number of levels building the TOS sector with fixed  $S_A$  is given as  $(2S_A + 1)^2$  (i.e. as for kagomé cylinders).

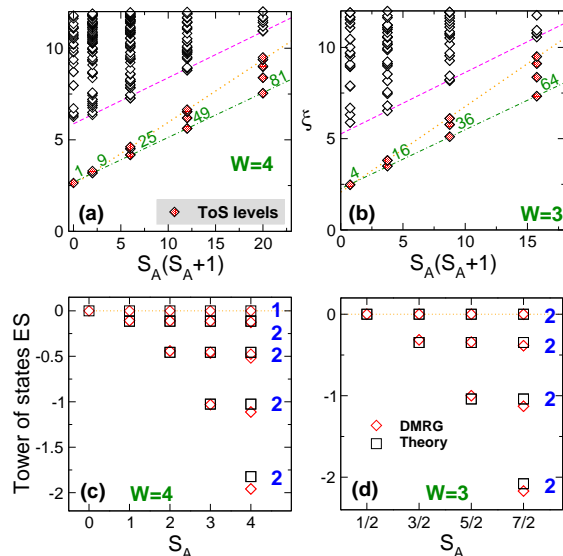


FIG. 6. ES of the kagomé  $J_1$ - $J_2$  Heisenberg model (KHA) on the torus. Data is DMRG at  $J_2/J_1 = -1$  and  $W = L/2 = 3$ ,  $W = L/2 = 4$  (respectively panels (a) and (b) in the Figure). The ES is for half of the torus: ES levels  $\xi$  plotted versus the subsystem spins  $S_A(S_A+1)$ . Filled rhombi denote the tower of states (TOS) ES levels. The numbers are the total numbers of TOS levels in each sector  $S_A$ . The dashed-dotted line highlights the linear behavior (with respect to  $S_A(S_A+1)$ ) of TOS levels. The dashed line marks the higher part of the ES. (c)(d) Enlarged view of TOS structures: TOS ES levels (same data as in (a)(b)) shifted by the value of the highest level (dotted line in (a)(b)) plotted versus  $S_A$ . The squares denote the (one parameter) fit to the expected result in the large volume limit (cf. formula (8)). The number of degenerate  $SU(2)$  multiplets is shown in blue.

The effective entanglement Hamiltonian  $\mathcal{H}_E$  describing the TOS structure is given by (8). This is demonstrated in Figure 6 (c,d). ES levels (only TOS levels are shown) are plotted versus the block spin  $S_A$ . Each ES tower (at fixed  $S_A$ ) was shifted by subtracting the contribution of the largest level (in that sector). Squares are one parameter fits to  $\alpha[(S_A^{z'})^2 + s_0]$  ( $\alpha$  is the fitting parameter, cf. section IV C), which give  $\alpha \approx 0.16$  and  $\alpha \approx 0.11$  for respectively  $W = 3$  and  $W = 4$ . It is instructive to observe that for kagomé cylinders one obtains  $\alpha \approx 0.17$  at  $W = 4$  (cf. section IV C). The reduction of  $\alpha$  (by a factor  $\approx 2$ ) has to be attributed to the two boundaries (between the subsystems).

## VI. CONCLUSIONS & OUTLOOK

In this Article we studied the *ground state* entanglement spectrum in  $SU(2)$ -broken phases. We considered the two dimensional  $J_1$ - $J_2$  Heisenberg model on both the triangular and kagomé lattice, restricting ourselves to antiferromagnetic(ferromagnetic)  $J_1(J_2)$  and  $J_2/J_1 = -1$ .

On both lattices the ground state of the model displays magnetic order (and  $SU(2)$  symmetry breaking, in the thermodynamic limit). This is associated with the appearance in the finite size (spin-resolved) energy spectrum of a special type of low-lying excitations, forming the so called tower of states (TOS). The TOS structure is divided from the higher part of the spectrum (at least for large system sizes) by an energy gap. The number of TOS energy levels in each spin sector  $S$  reflects the selected symmetry breaking pattern, and is given as  $(2S+1)^2$ .

In this work we demonstrated that this structure is reflected in the lower part of the *ground state* ES. Precisely, the ES exhibits families of low-lying levels, which are divided from the rest by an *entanglement gap*, and form a TOS-like structure. The number of TOS levels in a given (subsystem) spin sector  $S_A$  is  $(2S_A+1)^2$ , clearly reflecting the corresponding counting in the energy TOS. Moreover, finite size behaviors of low-lying ES levels can be understood in terms of the energy TOS. All these features can be expressed quantitatively as a mapping between the low-lying structure (excitations) of the physical Hamiltonian  $\mathcal{H}$  and of the entanglement Hamiltonian  $\mathcal{H}_E$  (expressed by formula (8)).

On the methodological side, our results suggest that entanglement (tower of states) spectroscopy, combined with  $SU(2)$ -symmetric DMRG, could be used as a tool for characterizing  $SU(2)$ -broken phases. Finally, we would like to mention that an intriguing research direction originating from this work would be to investigate how the TOS structure evolves in the  $J_1$ - $J_2$  kagomé Heisenberg model as the  $J_2 = 0$  point is approached. In particular, it would be interesting to characterize how the low-lying ES levels rearrange to reflect the onset of the  $Z_2$  spin liquid found in [54, 55].

## VII. ACKNOWLEDGMENTS

V.A. thanks Andreas Läuchli for very useful discussions and collaboration in a related project. V.A. and S.D. thank the MIPKs of Dresden, where this work was partly done, for the hospitality during the workshop “Entanglement Spectra in Complex Quantum Wavefunctions”. U.S. and S.D. acknowledge funding by DFG through NIM and SFB/TR 12.

[1] L. Amico, R. Fazio, A. Osterloh, and V. Vedral, Rev. Mod. Phys. **80**, 517 (2008). J. Eisert, M. Cramer, M. B. Plenio, Rev. Mod. Phys. **82**, 277 (2010).  
 [2] H. Li and F. D. M. Haldane, Phys. Rev. Lett. **101**, 010504 (2008).

[3] I. Peschel, V. Eisler, J. Phys. A: Math. Theor. **42** 504003 (2009).  
 [4] V. Alba, M. Haque and A. M. Läuchli, Phys. Rev. Lett. **108**, 227201 (2012).

- [5] L. Lepori, G. De Chiara, and A. Sanpera, *Phys. Rev. B* **87**, 235107 (2013).
- [6] P. Calabrese, A. Lefevre, *Phys. Rev. A* **78**, 032329 (2008).
- [7] G. De Chiara, L. Lepori, M. Lewenstein, and A. Sanpera, *Phys. Rev. Lett.* **109**, 237208 (2012).
- [8] A. M. Läuchli, arXiv:1303.0741 (2013) unpublished.
- [9] N. Regnault, B. A. Bernevig, F. D. M. Haldane, *Phys. Rev. Lett.* **103**, 016801 (2009). N. Bray-Ali, L. Ding, and S. Haas, *Phys. Rev. B* **80**, 180504(R) (2009). L. Fidkowski, *Phys. Rev. Lett.* **104**, 130502 (2010). A. M. Läuchli, E. J. Bergholtz, J. Suorsa, and M. Haque, *Phys. Rev. Lett.* **104**, 156404 (2010). R. Thomale, A. Sterdyniak, N. Regnault, and B. A. Bernevig, *Phys. Rev. Lett.* **104**, 180502 (2010). H. Yao and X. L. Qi, *Phys. Rev. Lett.* **105**, 080501 (2010). E. Prodan, T. L. Hughes, and B. A. Bernevig, *Phys. Rev. Lett.* **105**, 115501 (2010). F. Pollmann, A. M. Turner, E. Berg, M. Oshikawa, *Phys. Rev. B* **81**, 064439 (2010). M. Kargarian and G. A. Fiete, *Phys. Rev. B*, **82**, 085106 (2010). A. M. Turner, Y. Zhang, A. Vishwanath, *Phys. Rev. B*, **82**, 241102R (2010). Z. Papic, B. A. Bernevig, and N. Regnault, *Phys. Rev. Lett.* **106**, 056801 (2011). L. Fidkowski, T. S. Jackson and I. Klich, *Phys. Rev. Lett.* **107**, 036601 (2011). J. Dubail, and N. Read, *Phys. Rev. Lett.* **107**, 157001 (2011). J. Schliemann, *Phys. Rev. B* **83**, 115322 (2011). T. L. Hughes, E. Prodan, B. A. Bernevig, *Phys. Rev. B*, **83**, 245132 (2011). N. Regnault and B. A. Bernevig, *Phys. Rev. X* **1**, 021014 (2011). X. L. Qi, H. Katsura, and A. W. W. Ludwig, *Phys. Rev. Lett.* **108**, 196402 (2012). D. Poilblanc, N. Schuch, D. Perez-Garcia, and J.I. Cirac, *Phys. Rev. B* **86**, 014404 (2012); B. Swingle, and T. Senthil, *Phys. Rev. B* **86**, 045117 (2012). N. Schuch, D. Poilblanc, J. I. Cirac, and D. Perez-Garcia, arXiv:1210.5601 (unpublished). D. Poilblanc, and N. Schuch, *Phys. Rev. B* **87**, 140407 (2013). J. Schliemann, *New J. Phys.* **15**, 053017 (2013). Z. Liu, D. L. Kovrizhin, and E. J. Bergholtz, arXiv:1304.1323.
- [10] J. I. Cirac, D. Poilblanc, N. Schuch, and F. Verstraete, *Phys. Rev. B* **83**, 245134 (2011).
- [11] S. Tanaka, R. Tamura, H. Katsura, *Phys. Rev. B* **86**, 032326 (2012).
- [12] J. Lou, S. Tanaka, H. Katsura, N. Kawashima, *Phys. Rev. B* **84**, 245128 (2013).
- [13] A. J. A. James and R. M. Konik, *Phys. Rev. B* **87**, 241103(R) (2013) .
- [14] M. A. Metlitski and T. Grover, arXiv:1112.5166 unpublished.
- [15] V. Alba, M. Haque and A. M. Läuchli, *Phys. Rev. Lett.* **110**, 260403 (2013).
- [16] B. Bernu, C. Lhuillier, and L. Pierre, *Phys. Rev. Lett.* **69**, 2590 (1992).
- [17] B. Bernu, P. Lecheminant, C. Lhuillier, and L. Pierre, *Phys. Rev. B* **50**, 10048 (1994). I. Rousochatzakis, A. M. Läuchli, F. Mila, *Phys. Rev. B* **77**, 094420 (2008). I. Rousochatzakis, A. M. Läuchli, R. Moessner, *Phys. Rev. B* **85**, 104415 (2012).
- [18] P. Lecheminant, B. Bernu, L. Pierre, and C. Lhuillier, *Phys. Rev. B* **52**, 6647 (1995).
- [19] P. Lecheminant, B. Bernu, C. Lhuillier, L. Pierre, and P. Sindzingre, *Phys. Rev. B* **56**, 2521 (1997).
- [20] A. M. Läuchli, J. C. Domenge, C. Lhuillier, P. Sindzingre, and M. Troyer, *Phys. Rev. Lett.* **95**, 137206 (2005).
- [21] N. Shannon, T. Momoi, and P. Sindzingre, *Phys. Rev. Lett.* **96**, 027213 (2006).
- [22] P. Sindzingre, C. Lhuillier, *EPL* **88**, 27009 (2009).
- [23] K. Penc, and A. M. Läuchli, *Springer Series in Solid-State Sciences* **164**, 331 (2011).
- [24] C. Lhuillier, arXiv:cond-mat/0502464v1 (unpublished).
- [25] T. Oguchi, *J. Phys. Soc. Jpn. Suppl.* **52**, 183 (1883).
- [26] T. Jolicoeur and J. C. Le Guillou, *Phys. Rev. B* **40**, 2727 (1989).
- [27] S. J. Miyake, *J. Phys. Soc. Jpn.* **61**, 983 (1982).
- [28] R. R. P. Singh, D. A. Huse, *Phys. Rev. Lett.* **68**, 1766 (1992).
- [29] A. V. Chubukov, S. Sachdev, and T. Senthil, *J. Phys.: Condens. Matter* **6** (1994).
- [30] A. L. Chernyshev, M. E. Zhitomirsky, *Phys. Rev. B* **79**, 144416 (2009).
- [31] L. Capriotti, A. E. Trumper, and S. Sorella, *Phys. Rev. Rev. Lett.* **82**, 3899 (1999).
- [32] W. H. Zheng, J. O. Fjaerestad, R. R. P. Singh, R. H. McKenzie, and R. Coldea, *Phys. Rev. B* **74**, 224420 (2006).
- [33] S. R. White and A. L. Chernyshev, *Phys. Rev. Lett.* **99**, 127004 (2007).
- [34] J. B. Marston, and C. Zeng, *J. Appl. Phys.* **69**, 5962 (1991).
- [35] C. Zeng, and V. Elser, *Phys. Rev. B* **42**, 8436 (1990).
- [36] M. B. Hastings, *Phys. Rev. B* **63** 014413 (2000).
- [37] P. Nikolic, and T. Senthil, *Phys. Rev. B* **68**, 214415 (2003).
- [38] R. R. P. Singh, D. A. Huse, *Phys. Rev. B* **76**, 180407R (2007).
- [39] R. R. P. Singh, and D. A. Huse, *Phys. Rev. B* **77**, 144415 (2008).
- [40] Y. Iqbal, F. Becca, and D. Poilblanc, *New J. Phys.* **14**, 115031 (2012).
- [41] L. Messio, B. Bernu, and C. Lhuillier, *Phys. Rev. Lett.* **108**, 207204 (2012).
- [42] K. Yang, L. K. Warman, and S. M. Girvin, *Phys. Rev. Lett.* **70**, 2641 (1993).
- [43] M. Hermele et al., *Phys. Rev. B* **77**, 224413 (2008).
- [44] Y. Iqbal, F. Becca, and D. Poilblanc, *Phys. Rev. B* **84**, 020407 (2011).
- [45] Y. Ran et al., *Phys. Rev. Lett.* **98**, 117205 (2007).
- [46] S. Ryu et al., *Phys. Rev. B* **75**, 184406 (2007).
- [47] S. Sachdev, *Phys. Rev. B* **45**, 12377 (1992).
- [48] F. Wang and A. Vishwanath, *Phys. Rev. B* **74**, 174423 (2006).
- [49] Y. Lu, Y. Ran, and P. A. Lee, *Phys. Rev. B* **83**, 224413 (2011).
- [50] G. Misguich, D. Serban, and V. Pasquier, *Phys. Rev. Lett.* **89**, 137202 (2002).
- [51] H. C. Jiang, Z. Y. Weng, and D. N. Sheng, *Phys. Rev. Lett.* **101**, 117203 (2008).
- [52] Y. Huh, M. Punk, and S. Sachdev, *Phys. Rev. B* **84**, 094419 (2011).
- [53] V. Kalmeyer and R. B. Laughlin, *Phys. Rev. B* **39**, 11879 (1989).
- [54] S. Yan, D. Huse, and S. White, *Science* **332**, 1173 (2011).
- [55] S. Depenbrock, I. P. McCulloch, and U. Schollwöck, *Phys. Rev. Lett.* **109**, 067201 (2012).
- [56] H. C. Jiang, Z. Wang, and L. Balents, *Nature Phys.* **8**, 902 (2012).
- [57] S. R. White, *Phys. Rev. Lett.* **69**, 2863 (1992).
- [58] U. Schollwöck, *Rev. Mod. Phys.* **77**, 259 (2005).
- [59] U. Schollwöck, *Ann. Phys.* **326**, 96 (2011).
- [60] S. R. White, *Phys. Rev. Lett.* **77**, 3633 (1996).
- [61] S. R. White and D. J. Scalapino, *Phys. Rev. Lett.* **80**, 1272 (1998).
- [62] S. R. White and D. J. Scalapino, *Phys. Rev. Lett.* **81**, 3227 (1998).
- [63] E. M. Stoudenmire and S. R. White, *Ann. Rev. Cond. Mat. Phys.* **3**, 111 (2012).
- [64] P. W. Anderson, *Phys. Rev.* **86**, 694 (1952).
- [65] M. Gross, E. Sanchez-Velasco, and E. Siggia, *Phys. Rev. B* **40**, 11328 (1989).
- [66] D. S. Fisher, *Phys. Rev. B* **39**, 11783 (1989).
- [67] P. Azaria, B. Delamotte, and D. Mouhanna, *Phys. Rev. Lett.* **70**, 2483 (1993).
- [68] M. A. Metlitski and T. Grover, private communication.

- [69] A. B. Kallin, I. González, M. B. Hastings, and R. G. Melko, Phys. Rev. Lett. **103** 117203 (2009).
- [70] M. B. Hastings, I. González, A. B. Kallin, and R. G. Melko, Phys. Rev. Lett. **104** 157201 (2010).
- [71] H. F. Song, N. Laflorencie, S. Rachel, K. Le Hur, Phys. Rev. B **83**, 224410 (2011).